DOI: 10.1021/ic902496u

Inorganic Chemistry
Article

Combined Computational and Experimental Study of Uranyl(VI) 1:2 Complexation by Aromatic Acids

Jonas Wiebke,[†] Anna Weigand,[†] Daniel Weissmann,[†] Maja Glorius,[‡] Henry Moll,*[,‡] Gert Bernhard,[‡] and Michael Dolg*[,†]

[†]*Institut für Theoretische Chemie, Department für Chemie, Universität zu Köln, Greinstrasse 4, D-50939 Köln, Germany, and* [‡]*Forschungszentrum Dresden−Rossendorf e.V., Institut für Radiochemie, P.O. Box 510119, D-01314 Dresden, Germany*

Received December 16, 2009

The bis(salicylhydroxamato) and bis(benzohydroxamato) complexes of UO_2^{2+} in aqueous solution have been investigated in a combined experimental and computational effort using extended X-ray absorption fine structure and UV−vis spectroscopy and density functional theory (DFT) techniques, respectively. The experimentally unknown bis(benzoate) complex of UO_2^{2+} was investigated computationally for comparison. Experimental data indicate 5-fold UO_2^{2+} coordination with mean equatorial U−O distances of 2.42 and 2.40 Å for the salicyl- and benzohydroxamate systems, respectively. DFT calculations on microsolvated model systems $[UO_2L_2OH_2]$ indicate UO_2^{2+} η^2-chelation via the hydroxamate oxygen atoms in excellent agreement with experimental data; calculated complex stabilities support that UO_2^{2+} prefers hydroxamate over carboxylate coordination. The 414 nm absorption band of UO_2^{2+} in aqueous solution is blue-shifted to 390 and 386 nm upon complexation by salicyl- and benzohydroxamate, respectively. Calculated time-dependent DFT excitation energies of $[UO_2L_2OH_2]$, however, occasionally fail to reproduce accurately experimental UV−vis spectra, which are dominated by $UO_2^{2+} \leftarrow L^-$ charge-transfer contributions. We additionally show that the U^{VI} large-core pseudopotential approximation recently developed by some of the authors can routinely be applied for electronic structure calculations not involving uranium 5f occupations significantly different from U^{VI}.

1. Introduction

Relevance of actinide (and particularly uranium) chemistry comes mainly from nuclear weapon[1] and nuclear power technology.[2,3] Whereas large parts of the global strategic nuclear warhead arsenals[4] have been or are discussed to be subjected to dismantlement, nuclear energy will likely attract increasing interest in the short- and midterm future,[3] the latter both from the worldwide growing energy demand, as estimated[5] to increase from 473.5 EJ 2005 to ca. 680−910 EJ 2030 (6.0% and 4.9−6.1% supplied from nuclear energy, respectively) and from nuclear power's relative CO_2 neutrality. However, fundamental issues of, for example, long-term disposal strategies[6] for spent nuclear fuel and waste remain unresolved on political,[7] social,[8a,b] and, to some extent, scientific grounds. Much has been learned about actinide environmental and geochemistry,[9a,b] but reliable prediction of actinide migration in natural soil and groundwater, e.g., in a scenario of leaching from deep underground waste deposits, still is challenging, if at all feasible.

Today it is well known that the interaction of microorganisms such as bacteria and fungi with actinides and fission products, i.e., by biosorption, intracellular uptake, bioleaching, biomineralization, etc., of metal ions,[10a−c,11] is an important factor for environmental mobility. Considering bioleaching and mobilization from coordination by microbial

*To whom correspondence should be addressed. E-mail: m.dolg@uni-koeln.de; h.moll@fzd.de.

(1) O'Nions, K.; Pitman, R.; Marsh, C. *Nature* **2002**, *415*, 853–857.
(2) Choppin, G. R.; Rydberg, J.; Liljenzin, J.-O. *Radiochemistry and Nuclear Power*, 3rd ed.; Butterworth−Heinemann: Oxford, UK, 2001.
(3) Abu-Khader, M. M. *Prog. Nucl. Energy* **2009**, *51*, 225–235.
(4) Norris, R. S. *Bull. At. Sci.* **2006**, *62*, 64–67.
(5) *Energy, Electricity and Nuclear Power Estimates for the Period up to 2030*; IAEA: Vienna, 2006.
(6) Hoffman, D. C.; Choppin, G. R. *J. Chem. Educ.* **1986**, *63*, 1059–1064.
(7) Rogers, K. A. *Prog. Nucl. Energy* **2009**, *51*, 281–289.
(8) (a) Peters, E.; Slovic, P. *J. Appl. Social Psych.* **1996**, *26*, 1427–1453. (b) Slovic, P.; Flynn, J. H.; Layman, M. *Science* **1991**, *254*, 1603–1607.
(9) (a) Choppin, G. R. *J. Nucl. Radiochem. Sci.* **2005**, *6*, 1–5. (b) Murphy, W. M.; Shock, E. L. In *Environmental Aqueous Geochemistry of Actinides*; Burns, P. C.; Finch, R., Eds.; Reviews in Mineralogy, Vol. *38*; Mineralogical Society of America: Washington, DC, 1999.
(10) (a) Suzuki, Y.; Banfield, J. F. In *Geomicrobiology of Uranium*; Burns, P. C.; Finch, R., Eds.; Reviews in Mineralogy, Vol. *38*; Mineralogical Society of America: Washington, DC, 1999. (b) Renshaw, J. C.; Lloyd, J. R.; Livens, F. R. *C. R. Chim.* **2007**, *10*, 1067–1077. (c) Simonoff, M.; Sergeant, C.; Poulain, S.; Pravikoff, M. S. *C. R. Chim.* **2007**, *10*, 1092–1107.
(11) King, F. *Corrosion* **2009**, *65*, 233–251.

 Published on Web 06/15/2010

"bioligands", siderophores of the pyoverdin type secreted by *Pseudomonas* spp. under iron-deficient conditions are an important class to consider[12] due to their known high potential to bind actinides,[13a−d] particularly Th^{IV}, U^{VI}, U^{IV}, Np^{V}, and Cm^{III}. Pyoverdins[14] are low-molecular chromopeptides that bind Fe^{3+} via catecholate and hydroxamate functionalities at their peptide backbone and (1*S*)-5-amino-2,3-dihydro-8,9-dihydroxy-1*H*-pyrimido[1,2*a*]quinoline-1-carboxylic acid chromophore moieties, respectively,[15] and binding of UO_2^{2+} is most likely analogous. It is thus reasonable to model UO_2^{2+}−pyoverdin interactions by simpler U^{VI}−catecholate and −hydroxamate systems, and a number of studies[16a−i,17−21] have been carried out mainly from an extraction chemistry point of view.[16a−h] Detailed structure and stability data are, however, scarce.

Recently, some of the authors reported UV−vis,[19] extended X-ray absorption fine structure (EXAFS),[21] and time-resolved laser-induced fluorescence (TRLF) spectroscopic investigations[20] of U^{VI}−salicylhydroxamic acid, −benzohydroxamic acid, and −benzoic acid systems, as well as density functional theory (DFT) electronic structure calculations[21] of simple model systems $[UO_2L(OH_2)_3]^+$, L^- being salicylhydroxamate, $HOC_6H_4CONHO^-$, benzohydroxamate, $C_6H_5CONHO^-$, and benzoate, $C_6H_5CO_2^-$ (sha^-, bha^-, and ba^-, respectively). Generally, the hydroxamate ligands coordinate UO_2^{2+} with mean U−O distances of 2.41 Å,[21] forming complexes with UO_2^{2+}-to-ligand ratios of both 1:1 and 1:2.[17,19−21] In the benzoate system experimentally only a 1:1 complex could be determined so far, and stimulated by theoretical computations, investigations are in progess to verify the formation of a 1:2 U^{VI}−benzoate species. TRLF spectroscopic stability constants[20] log β of 17.23 and 35.0 for the 1:1 and 1:2 sha and of 7.94 and 16.07 for the 1:1 and 1:2 bha systems, respectively, agree with recent UV−vis[19] but not with older potentiometric investigations,[17] whereas, qualitatively, 1:2 complexes are found to be stronger than 1:1, and sha^- to be stronger than bha^- complexes from all studies.[17,19,20] Both sha^- and bha^- blue-shift the UO_2^{2+} absorption maximum to 402 and 401 nm upon 1:1 complexation, respectively.[19] However, EXAFS structure parameters are necessarily one-dimensional and must be regarded as averages over both systems of different composition, i.e., free UO_2^{2+}, mono- and bishydroxamato complexes in aqueous solution, and systems with different but somewhat similar ligands, i.e., oxygen donators sha^- or bha^- and OH_2. DFT calculations[21] indicate η^2-coordination of UO_2^{2+} via the hydroxamic acid oxygen atoms in the UO_2^{2+} equatorial plane, as found for related[18] and similar systems,[22a−d] but in view of the EXAFS samples' somewhat complicated composition[21] the $[UO_2L(OH_2)_3]^+$ structure model is clearly limited.

As we believe that meaningful modeling of complex systems and processes, e.g., actinide complexation by pyoverdin-type siderophores, must, in the first place, imply detailed understanding of the model, we decided to extend our previous investigations[19−21] of U^{VI}−hydroxamates and −benzoates. Therefore, we present here molecular structure information from both EXAFS spectroscopy and DFT calculations, calculated relative stabilities, and experimental UV−vis and calculated time-dependent DFT (TD-DFT) excitation spectra, focusing on the bis(hydroxamato)- and bis(benzoate)dioxouranium(VI) complexes in aqueous solution. As a computational add-on we also show that all electronic structure calculations can, without significant loss of accuracy, also be carried out employing the scalar-relativistic large-core pseudopotential approximation for U^{VI} recently developed by some of the authors.[23]

2. Experimental Section

2.1. Solutions and Reagents. A stock solution of 0.1 M uranyl perchlorate was prepared by dissolving $UO_3 \cdot 0.77H_2O$ in 0.3 M $HClO_4$ and analyzed by inductively coupled plasma mass spectrometry. Salicylhydroxamic acid (Sigma-Aldrich, Germany), benzohydroxamic acid, and sodium perchlorate (Merck, Germany) were of analytical grade; all other reagents were provided by Merck, Germany. pH adjustments were made with $HClO_4$ and NaOH. pH measurements (accuracy: 0.05 units) were carried out using a BlueLine 16 pH glass electrode (Schott-Geräte GmbH, Mainz, Germany) calibrated with standard buffer solutions and a WTW pH540GLP pH meter (WTW, Weinheim, Germany). For all experiments the Na^+ concentration was kept at 0.1 M by adding $NaClO_4$. EXAFS measurements were performed at fixed sha^- and bha^- concentrations of 8×10^{-3} M within a pH range of 2.5−4.0 and UO_2^{2+} concentrations of 5×10^{-4} and 1×10^{-3} M, respectively.

2.2. Extended X-ray Absorption Fine Structure Measurements. EXAFS measurements were carried out at the Rossendorf Beamline (ROBL) BM20 at the European Synchrotron Radiation Facility.[24] All measurements were done at room

(12) Kalinowski, B. E.; Oskarsson, A.; Albinsson, Y.; Alinger, J.; Ödegaard-Jensen, A.; Andlid, T.; Pedersen, K. *Geoderma* **2004**, *112*, 117–194.
(13) (a) Moll, H.; Glorius, M.; Bernhard, G.; Johnsson, A.; Pedersen, K.; Schäfer, M.; Budzikiewicz, H. *Geomicrobiol. J.* **2008**, *25*, 157–166. (b) Moll, H.; Johnsson, A.; Schäfer, M.; Pedersen, K.; Budzikiewicz, H.; Bernhard, G. *Biometals* **2008**, *21*, 219–228. (c) Bouby, M.; Billard, I.; Maccordick, H. J. *Czech. J. Phys.* **1999**, *49*, 769–772. (d) Moll, H.; Glorius, M.; Johnsson, A.; Schäfer, M.; Budzikiewicz, H.; Pedersen, K.; Bernhard, G. *Radiochim. Acta* **2010**, accepted.
(14) Budzikiewicz, H. *Fortschr. Chem. Org. Naturst.* **2004**, *87*, 83–237.
(15) Albrecht-Gary, A.-M.; Blanc, S.; Rochel, N.; Ocaktan, A. Z.; Abdallah, M. A. *Inorg. Chem.* **1994**, *33*, 6391–6402.
(16) (a) Tkac, P.; Matteson, B.; Bruso, J.; Paulenova, A. *J. Radioanal. Nucl. Chem.* **2008**, *227*, 31–36. (b) Gong, C.-M. S.; Poineau, F.; Czerwinski, K. R. *Radiochim. Acta* **2007**, *95*, 439–450. (c) Boulet, B.; Bouvier-Capely, C.; Cossonnet, C.; Cote, G. *Solvent Extr. Ion Exch.* **2006**, *24*, 319–330. (d) Agrawal, Y. K.; Shah, G.; Vora, S. B. *J. Radioanal. Nucl. Chem.* **2006**, *270*, 453–459. (e) Pal, S.; Ramachandhran, V.; Prabhakar, S.; Tewari, P. K.; Sudersanan, M. *J. Marcomol. Sci. A* **2006**, *43*, 735–747. (f) Jain, V. K.; Pillali, S. H.; Pandya, R. A.; Agrawi, Y. K.; Shrivastav, P. S. *Talanta* **2005**, *65*, 466–475. (g) Leydier, A.; Lecercle, D.; Pellet-Rostaing, S.; Favre-Reguillon, A.; Taran, F.; Lemaire, M. *Tetrahedron* **2008**, *64*, 6662–6669. (h) Sawicki, M.; Siauge, J. M.; Jacopin, C.; Moulin, C.; Bailly, T.; Burgada, R.; Meunier, S.; Baret, P.; Pierre, J. L.; Taran, F. *Chem.—Eur. J.* **2005**, *11*, 3689–3697. (i) Hay, B. P.; Uddin, J.; Firman, T. K. *Polyhedron* **2004**, *23*, 145–154.
(17) Khairy, E. M.; Shoukry, M. M.; Khalil, M. M.; Mohamed, M. M. A. *Transition Met. Chem.* **1996**, *21*, 176–180.
(18) Boulet, B.; Joubert, L.; Cote, G.; Bouvier-Capely, C.; Cossonnet, C.; Adamo, C. *Inorg. Chem.* **2008**, *47*, 7983–7991.
(19) Glorius, M.; Moll, H.; Bernhard, G. *Radiochim. Acta* **2007**, *95*, 151–157.
(20) Glorius, M.; Moll, H.; Geipel, G.; Bernhard, G. *J. Radioanal. Nucl. Chem.* **2008**, *277*, 371–377.
(21) Wiebke, J.; Moritz, A.; Glorius, M.; Moll, H.; Bernhard, G.; Dolg, M. *Inorg. Chem.* **2008**, *47*, 3150–3157.
(22) (a) Ray, R. S.; Krüger, S.; Rösch, N. *Dalton Trans.* **2009**, 3590–3598. (b) Ikeda, A.; Henning, C.; Tsushima, S.; Takao, K.; Ikeda, Y.; Scheinost, A. C.; Bernhard, G. *Inorg. Chem.* **2007**, *46*, 4212–4219. (c) de Jong, W. A.; Apra, E.; Windus, T. L.; Nichols, J. A.; Harrison, R. J.; Gutowski, K. E.; Dixon, D. A. *J. Phys. Chem. A* **2005**, *109*, 11568–11577. (d) Hemmingsen, L.; Amara, P.; Ansoborlo, E.; Field, M. J. *J. Phys. Chem. A* **2000**, *104*, 4095–4101.
(23) Moritz, A.; Dolg, M. *Theor. Chem. Acc.* **2008**, *121*, 297–306.
(24) Matz, W.; Schell, N.; Bernhard, G.; Prokert, F.; Reich, T.; Claussner, J.; Oehme, W.; Schlenk, R.; Dienel, S.; Funke, H.; Eichhorn, F.; Betzl, M.; Prohl, D.; Strauch, U.; Huttig, G.; Krug, H.; Neumann, W.; Brendler, V.; Reichel, P.; Denecke, M. A.; Nitsche, H. *J. Synchrotron Radiat.* **1999**, *6*, 1076–1085.

temperature using a water-cooled Si(111) double-crystal monochromator in channel-cut mode (5−35 keV). Uranium L(III) spectra were recorded either in fluorescence mode, using a 13-element germanium solid-state detector, or in transmission mode, using argon-filled ionization chambers. For energy calibration of the spectra the K-edge spectrum of a yttrium metal foil (first inflection point: 17038 eV) was recorded simultaneously. The threshold energy of the U L(III)-edge was defined as the root of the second derivative of the averaged spectra. All spectra were processed using the Sixpack/SamView v. 0.59 data analysis[25] and WinXAS v. 3.1 programs.[26] Theoretical backscattering phases and amplitude functions were calculated using the FEFF8 code[27] for a 23-atom cluster using atomic positions of $UO_2(CH_3COO)_2 \cdot 2H_2O$[28a] and for the 42-atom cluster $[UO_2NO_3(C_7H_4O_3)]_2$ using atomic positions of $[UO_2NO_3(C_7H_4O_3)(C_7H_{11}N_2)]_2$.[28b] Model calculations included the multiple scattering path U−O (axial, four-legged). The amplitude factor S_0^2 was set constant to 1.0 for all fits.

3. Computational Details

All calculations were carried out at the B3LYP-DFT level of theory,[29a−f] using the TURBOMOLE v. 5.10 system of programs.[30a,b] For U a 5f-in-valence small-core relativistic pseudopotential[31a] with the (14s13p10d8f)/[10s9p5d4f] segmented-contracted valence-only basis set of Cao and Dolg[31b] has been used, if not stated otherwise; for comparison, the recently adjusted hexavalent U^{VI} large-core relativistic pseudopotential[23] with the corresponding (7s6p5d2f1g)/[6s5p4d2f1g] valence-only basis set[23] has been used. Put in a somewhat simplified way, in the small-core and large-core pseudopotential (SPP and LPP) approximations the 60 and 78 electrons with main quantum numbers $n \leq 4$ and $n \leq 5$ are included in the PP core, giving rise to U^{VI} $5s^25p^65d^{10}5f^06s^26p^6$ effective 26-electron systems and U^{VI} $6s^26p^6$ effective eight-electron systems, respectively. For all other atoms the TZP basis sets of Schäfer et al.[32a] have been used. Except for the UO_2^{2+} O atoms, all O and N TZP basis sets were augmented by one diffuse s-, p-, and d-function with exponents from the corresponding aug-cc-pVDZ basis sets of Dunning Jr. et al.[33] (exponents O: $\alpha_s = 0.0790$, $\alpha_p = 0.0686$, $\alpha_d = 0.3320$; N: $\alpha_s = 0.0612$, $\alpha_p = 0.0561$, $\alpha_d = 0.2300$). As DFT exchange−correlation energies are numerically integrated on element-specific grids[30b] in TURBOMOLE, and since no U grid is implemented in v. 5.10, all calculations were carried out employing the tungsten dynamic m5 grid.[30b] Total energies were converged to 10^{-9} au. Molecular structures have been optimized without symmetry constraints to gradient norms less than 10^{-3} au using TURBOMOLE's STATPT algorithm. The minimum nature of all potential energy hypersurface stationary points has been confirmed via analytical frequency analysis using the TURBOMOLE AOFORCE module;[30b] B3LYP-DFT vibrational zero-point energies (ZPEs) have been scaled by 0.972.[34]

Single-point energy calculations with the conductor-like screening model COSMO[35a,b] have been carried out for infinite continuum permittivity, using solute cavities constructed from the default parameter set and the COSMO-RS atomic radii[36] of 1.30, 2.00, 1.83, and 1.72 Å for H, C, N, and O, respectively, and 2.00 Å for U.[37] Starting from canonical Kohn−Sham and Hartree−Fock orbitals optimized in the COSMO potential, electronic excitation energies have been calculated within the adiabatic approximation of TD-DFT[38a] considering the 100 energetically lowest singlet excitations and at the resolution-of-identity configuration interaction singles, RI-CIS, and RI-CIS with perturbative double corrections, RI-CIS(D), levels of theory,[38b] using the auxiliary basis of Schimmelpfennig for U[31c] and of Weigend et al. for H, C, N, and O.[32b] For every calculated spectral line, one Gaussian function $a_0 \exp(-b(\lambda - \lambda_0)^2)$ was used to represent the contribution to the continuous spectrum; a_0 is the oscillator strength, λ_0 is the excitation wavelength, and $b = 0.005$ is a broadening parameter. Exemplary SPP calculations using second-order RI Møller−Plesset perturbation theory, RI-MP2,[38c] have been carried out with the same basis sets,[31c,32b] freezing orbitals with energies below −10 au.

4. Results and Discussion

4.1. EXAFS Structure Parameters. Figure 1 shows the U L(III) edge k^3-weighted EXAFS spectra and Fourier transforms (FTs) of the U^{VI}−salicylhydroxamate and −benzohydroxamate samples and, for comparison, of a sample containing the uncomplexed "free" UO_2^{2+} ion.[21] Albeit small, differences in the EXAFS oscillations of the sha^-- and bha^--containing samples' with respect to the "free" UO_2^{2+} ion sample's EXAFS function in the 6−9 $Å^{-1}$ k range are attributed to complex formation, i.e., to replacement of OH_2 from the UO_2^{2+} solvation shell by sha^- and bha^- ligands, respectively, retaining the U^{VI} equatorial coordination number of ca. 5 ± 1. Consequently, differences of the EXAFS FTs and, thus, of the structure parameters obtained and given in Table 1 are small, too. Mean apical and equatorial U−O distances are 1.78 and 2.42 Å for the sha and 1.77 and 2.40 Å for the bha system, respectively, and do not differ significantly from the free, i.e., solvated, UO_2^{2+} U−O distances of 1.77 and 2.42 Å within the experimental error of ca. ± 0.01 Å. Generally, EXAFS U−O distances are also very similar to those recently reported[21] for otherwise analogous samples with larger relative proportions of the 1:1 complexes. Because UO_2^{2+}−OH_2 distances are typically larger than UO_2^{2+}−O distances involving η^2-hydroxamate[18,21] and η^1- and η^2-carboxylate oxygen atoms,[22a−d,21] one could have expected smaller mean U−O distances as

(25) Webb, S. M. *Phys. Scr.* **2005**, *115*, 1011–1014.
(26) Ressler, T. *J. Synchrotron Radiat.* **1998**, *5*, 118–122.
(27) Ankudinov, A. L.; Ravel, B.; Rehr, J. J.; Conradson, S. D. *Phys. Rev. B* **1998**, *58*, 7565–7576.
(28) (a) Howatson, J.; Grev, D. M.; Morosin, B. *J. Inorg. Nucl. Chem.* **1975**, *37*, 1933–1935. (b) Nassimbeni, L. R.; Rodgers, A. L.; Haigh, J. M. *Inorg. Chim. Acta* **1976**, *20*, 149–153.
(29) (a) Dirac, P. A. M. *Proc. Cambr. Philos. Soc.* **1930**, *26*, 376–385. (b) Slater, J. C. *Phys. Rev.* **1951**, *81*, 385–390. (c) Vokso, S. H.; Wilk, L.; Nusair, M. *Can. J. Phys.* **1980**, *58*, 1200–1211. (d) Becke, A. D. *Phys. Rev. A* **1988**, *38*, 3098–3100. (e) Lee, C.; Yang, W.; Parr, R. G. *Phys. Rev. B* **1988**, *37*, 785–789. (f) Becke, A. D. *Chem. Phys.* **1993**, *98*, 5684–5652.
(30) (a) Ahlrichs, R.; Bär, M.; Häser, M.; Horn, H.; Kölmel, C. *Chem. Phys. Lett.* **1989**, *162*, 165–169. (b) Treutler, O.; Ahlrichs, R. *J. Chem. Phys.* **1995**, *102*, 346–354.
(31) (a) Küchle, W.; Dolg, M.; Stoll, H.; Preuss, H. *J. Chem. Phys.* **1994**, *100*, 7535–7542. (b) Cao, X.; Dolg, M. *J. Mol. Struct.* **2004**, *673*, 203–209. (c) Armbruster, M. K.; Schimmelpfennig, B.; Plaschke, M.; Roth, J.; Denecke, M. A.; Klenze, R. *J. Electron Spectrosc. Relat. Phenom.* **2009**, *169*, 51–56.
(32) (a) Schäfer, A.; Huber, C.; Ahlrichs, R. *J. Chem. Phys.* **1994**, *100*, 5829–5835. (b) Weigend, F.; Häser, M.; Patzelt, H.; Ahlrichs, R. *Chem. Phys. Lett.* **1998**, *294*, 143–152.
(33) Kendall, R. A.; Dunning, T. H., Jr.; Harrison, R. J. *J. Chem. Phys.* **1992**, *96*, 6796–6808.
(34) Neugebauer, J.; Hess, B. A. *J. Chem. Phys.* **2003**, *118*, 7215–7225.
(35) (a) Klamt, A.; Schüürmann, G. *J. Chem. Soc., Perkin Trans.* **1993**, *2*, 799–805. (b) Schäfer, A.; Klamt, A.; Sattel, D.; Lohrenz, J. C. W.; Eckert, F. *Phys. Chem. Chem. Phys.* **2000**, *2*, 2187–2193.
(36) Klamt, A.; Jonas, V.; Bürger, T.; Lohrenz, J. C. W. *Phys. Chem. A* **1998**, *102*, 5074–5085.
(37) Gutowski, K. E.; Dixon, D. A. *J. Phys. Chem. A* **2006**, *110*, 8840–8856.
(38) (a) Bauernschmitt, R.; Ahlrichs, R. *Chem. Phys. Lett.* **1996**, *256*, 454–464. (b) Hättig, C.; Weigend, F. *J. Chem. Phys.* **2000**, *113*, 5154–5161. (c) Weigend, F.; Häser, M. *Theor. Chem. Acc.* **1997**, *97*, 331–340.

compared to both free UO_2^{2+} and those recently reported.[21] On the other hand, $UO_2^{2+}-O$ distances involving η^2-hydroxamate O atoms should be larger for 1:2 than for 1:1 complexes from larger steric $L^- - L^-$ and $L^- - OH_2$ interaction and might well approach $UO_2^{2+}-OH_2$ distances of 2.42 Å. However, support of this interpretation is clearly limited from the present data set. Therefore, no attempt will be made here to draw any conclusion other than, at first, EXAFS U−O distances are very similar for free UO_2^{2+} and UO_2^{2+} complexed by sha^- and bha^- in aqueous solution and, second, that the one-dimensional EXAFS structure

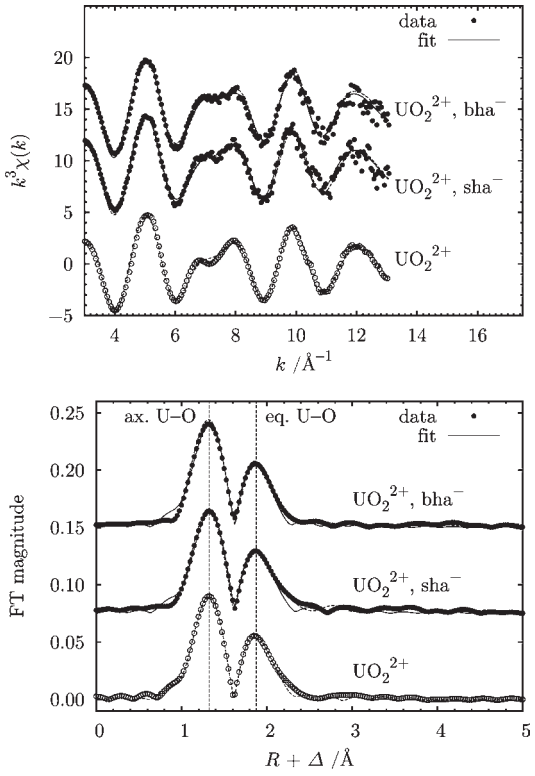

Figure 1. U L_{III}-edge k^3-weigthed EXAFS spectra and Fourier transforms of the sha and bha systems and of a "free" UO_2^{2+} sample,[21] including the best theoretical fits.

model is clearly limited in its explanatory power when it comes to the discrimination of systems with different, but somewhat similar O-donor ligands.

4.2. Calculated Molecular Structures. If not stated otherwise, all calculations refer to the SPP computational scheme as discussed in section 3.

4.2.1. Bis(salicylhydroxamato)-, Bis(benzohydroxamato)-, and Bis(benzoato)dioxouranium(VI). The straightforward consideration of systems of composition $[UO_2L_2]$, L^- being sha^- or bha^-, gives rise to quite a large number of possible coordination isomers, and it is not clear *a priori* which one or which ones are the most appropriate representations of the actual systems observed experimentally. In the first place, considering η^2-chelating modes only, one can model UO_2^{2+} coordination via the hydroxamic acid oxygen and via the hydroxamic acid oxygen and nitrogen atoms, i.e., via η^2-[O,O] and -[N,O] modes, whereas in the sha^- case one can model additional η^2-[O,O′] and -[N,O′] modes, both involving the phenolic O′ atom. Given a pair of such modes, in a $[UO_2L_2]$ system both *syn*- and *anti*-like relative L^- orientations are reasonable (cf. Figure 2).[39] To limit the number of calculations to be carried out, we note that it appears to be generally accepted[18,19] and has been shown within our computational protocol[21] that, at least for UO_2^{2+} coordination, η^2-[O,O] is the favored coordination mode of both sha^- and bha^-. Calculated η^2-[O,O] *syn*- and *anti*-$[UO_2sha_2]$ interatomic distances $d \leq 2.75$ Å differ by at most 0.011 Å, and total energies of both isomers differ by much less than 1 kJ mol^{-1}. Thus, both isomers appear to be equally thermally accessible, pointing to the necessity of population-weighted averaging, but both are very similar in terms of structure parameters that can be compared to experimental, i.e., EXAFS data, in a meaningful way. We therefore limit our computational model of the $[UO_2L_2]$ systems to the η^2-[O,O] *anti*-$[UO_2L_2]$ isomers, which, moreover, simplifies microsolvation of the UO_2^{2+} fragment as discussed below.

Generally, all systems considered are quite similar in terms of structure parameters, the sha and bha systems being more similar among each other than to the ba system (cf. Table 2). Apical UO_2^{2+} U−O distances are largely independent of L^-, differing by 0.012 Å at most, and are elongated by at most 0.093 Å compared to $d_{U-O} = 1.698$ Å

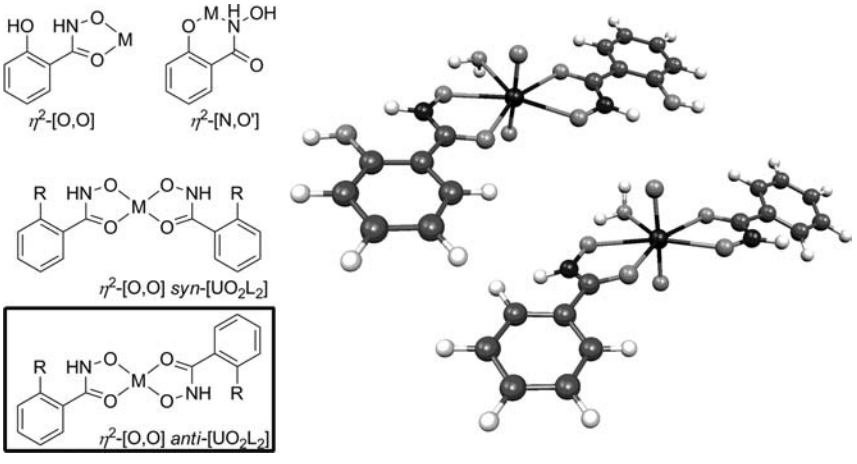

Figure 2. Schematic representation of the salicylhydroxamate ligand's η^2-[O,O] and η^2-[N,O′] coordination modes and of the η^2-[O,O] mode *syn*- and *anti*-like $[UO_2L_2]$ coordination isomers, R = OH for sha^- and R = H for bha^-. M is UO_2^{2+}. Three-dimensional molecular structures of $[UO_2L_2OH_2]$, derived from the η^2-[O,O] mode *anti*-like parent $[UO_2L_2]$ systems, have been calculated within the B3LYP-DFT SPP computational scheme.

Table 1. EXAFS Sample Composition and EXAFS Data, i.e., Coordination Numbers $N \pm 15\%$, Interatomic Distances $R \pm 0.01$ Å in Å, Debye−Waller Factors σ^2 in Å^2, and Energy Thresholds ΔE_0 in eV[a]

ligand	U^{VI} speciation	shell	N	R	σ^2	ΔE_0
	0.05 M UO_2^{2+}, pH 2.0 (100% UO_2^{2+})	ap.	1.9	1.77	0.0016	10.5
		eq.	5.0	2.42	0.0068	
sha^-	0.0005 M UO_2^{2+}, 0.008 M sha^-, pH 3.0	ap.	2.2	1.78	0.0026	13.4
	76% $[UO_2sha_2]$, 12% $[UO_2sha]^+$, 12% UO_2^{2+}	eq.	4.7	2.42	0.0063	
bha^-	0.001 M UO_2^{2+}, 0.008 M bha^-, pH 4.0	ap.	2.3	1.77	0.0027	12.3
	90% $[UO_2bha_2]$, 8% $[UO_2bha]^+$, 2% UO_2^{2+}	eq.	4.8	2.40	0.0064	

[a] U^{VI} speciation was done using the SOLGASWATER program.[45] The "free" UO_2^{2+} sample's data have been reproduced from ref 21 for comparison.

Table 2. B3LYP-DFT-Calculated $[UO_2L_2]$ and UO_2^{2+} Molecular Structure Parameters from the SPP and LPP Computational Scheme[a]

	$[UO_2sha_2]$		$[UO_2bha_2]$		$[UO_2ba_2]$		UO_2^{2+}	
	SPP	LPP	SPP	LPP	SPP	LPP	SPP	LPP
d_{U-O}	1.782, 1.782	1.734, 1.734	1.781, 1.781	1.732, 1.732	1.770, 1.770	1.720, 1.720	1.698, 1.698	1.643, 1.643
d_{U-OC}	2.417, 2.416	2.379, 2.379	2.423, 2.423	2.386, 2.386	2.391, 2.391, 2.391, 2.391	2.366, 2.366, 2.366, 2.366		
d_{U-ON}	2.322, 2.323	2.310, 2.310	2.324, 2.324	2.312, 2.312				
mean eq. d_{U-O}	2.370	2.345	2.374	2.349				
θ_{O-U-O}	180.0	180.0	180.0	180.0	180.0	180.0	180.0	180.0
$\theta_{CO-U-ON}$	66.7, 66.7	67.3, 67.3	66.8, 66.8	67.4, 67.4				
$\theta_{CO-U-OC}$					54.8, 54.8	55.4, 55.4		
$\lvert\theta_{NO-U-OC-C}\rvert$	21.6, 21.6	22.5, 22.5	21.8, 21.8	22.6, 22.6				
$\lvert\theta_{N-C-C-CH}\rvert$	1.2, 0.6	1.2, 1.1	25.8, 25.8	25.6, 25.7				

[a] Interatomic distances and angles are given in Å and deg, respectively.

calculated for free UO_2^{2+}. Both the sha and bha systems' equatorial U−O distances are very similar, d_{U-OC} being slightly larger than d_{U-ON} by 0.094 and 0.099 Å for sha^- and bha^-, respectively. The ba system's d_{U-OC} of 2.391 Å is in between the hydroxamate U−O distances, but larger than the sha and bha systems' averaged equatorial U−O distances of 2.370 and 2.374 Å, respectively. In all cases L^- coordination takes place in the UO_2^{2+} equatorial plane. Both hydroxamate ligands are tilted outside the CO−U−ON plane, as judged by the dihedral angles $|\theta_{NO-U-OC-C}|$ of 21.6° and 21.8° for sha^- and bha^-, respectively, whereas, as also found for the free sha^- and bha^- ligands, the bha^- ligand itself is twisted internally by $|\theta_{N-C-C-CH}| = 25.8°$ in $[UO_2bha_2]$, as compared to 1.2° for the sha^- ligand. The sha^- and bha^- ligands have almost identical bite angles θ of 66.7° and 66.8°, respectively, whereas ba^- has a significantly smaller bite of $\theta = 54.8°$.

Both the sha and bha systems' apical U−O distances of 1.782 and 1.781 Å perfectly match their experimental counterparts of 1.78 and 1.77 Å, respectively; the average equatorial U−O distances of 2.370 and 2.374 Å, respectively, compare qualitatively well but, in fact, underestimate experimental EXAFS values of 2.42 and 2.40 Å by ca. 0.05 and 0.03 Å. Clearly, agreement with experimental EXAFS data must here be attributed to somewhat fortuitous error cancellations from both the neglect from discrete and bulk solvation effects and systematic DFT errors.

The LPP computational scheme essentially provides the same global picture as discussed above. Quantitatively, U-involving interatomic distances of UO_2^{2+} and the $[UO_2L_2]$ sha, bha, and ba systems are consistently smaller by at most 0.050, 0.049, 0.048, and 0.050 Å, respectively; deviations of angular parameters (at most 1.37°, 1.42°, and 1.01° for the sha, bha, and ba systems) are less pronounced and less systematic. As expected, within the otherwise identical computational protocol, ligand-related structure parameters, such as dihedral angles, are largely unaffected.

4.2.2. Modeling Solvation: Monoaqua-bis(salicylhydroxamato)-, -bis(benzohydroxamato)-, and -bis(benzoato)dioxouranium(VI). Following previous work,[21] the solvation of UO_2^{2+} and $[UO_2L_2]$ was modeled in a hybrid-type fashion, i.e., considering discrete solute−solvent interaction both by including a small number of OH_2 molecules around the system of interest and by correcting for long-range conformation-averaged interactions by employing COSMO for single-point energy calculations. Because of computational feasibility and because the UO_2^{2+} fragment was expected to be the most strongly affected by solvation, a complete solvation shell was modeled only for the UO_2^{2+} fragment; that is, in $[UO_2L_2]$ no discrete L^- solvation was considered. The number x' of OH_2 ligands in the $[UO_2L_2]$ equatorial plane was deduced of considering the rearrangements $[UO_2L_2(OH_2)_{x-1}\cdot OH_2] \rightarrow [UO_2L_2(OH_2)_x]$, with $[UO_2L_2(OH_2)_{x-1}\cdot OH_2]$ having $x - 1$ OH_2 ligands in the first and one OH_2 ligand in the second UO_2^{2+} solvation shell. Then, x' is the largest x for this particular rearrangement that still gives negative reaction energies. Within our general computational protocol, from optimal molecular structures outside of and single-point energies within the COSMO potential, $[UO_2sha_2OH_2\cdot OH_2]$ was found to be favored with respect to $[UO_2sha_2(OH_2)_2]$ by 17.8 kJ mol^{-1} including ZPE corrections. Therefore, in line with the experimental EXAFS data, x' equals 1; note that from η^2-[O,O] *anti*-$[UO_2sha_2]$ one can construct only one distinct $[UO_2sha_2OH_2]$ system, as opposed to the *syn*-like isomer. We point out that this does not disagree with the recent

(39) Moreover, one formally had to consider two distinct sha^- rotamers differing by the relative orientations of the hydroxamic acid and phenolic OH functionalities, as both give two distinct potential energy hypersurface minima. For the isolated sha^- system, however, the rotamer with the $NH-O^-$ unit facing the phenolic OH functionality was found to be more stable by 21.0 kJ mol^{-1}, and we assume this to hold for all UO_2^{2+}-coordinating scenarios considered.

Table 3. Calculated B3LYP-DFT $[UO_2L_2OH_2]$ and $[UO_2(OH_2)_5]^{2+}$ molecular structure parameters from the SPP and LPP computational scheme, and U^{VI} Mulliken f populations n_f[a]

	$[UO_2sha_2OH_2]$		$[UO_2bha_2OH_2]$		$[UO_2ba_2OH_2]$		$[UO_2(OH_2)_5]^{2+}$	
	SPP	LPP	SPP	LPP	SPP	LPP	SPP	LPP
d_{U-O}	1.786, 1.786	1.740, 1.734	1.781, 1.784	1.736, 1.736	1.772, 1.776	1.728, 1.723	1.748, 1.748	1.747, 1.747
d_{U-OC}	2.402, 2.454	2.373, 2.421	2.412, 2.464	2.379, 2.427	2.386−2.482	2.362−2.455		
d_{U-ON}	2.325, 2.434	2.312, 2.420	2.326, 2.436	2.318, 2.427				
d_{U-OH}	2.600	2.563	2.594	2.558	2.554	2.518	2.495−2.497	2.216−2.241
mean eq. d_{U-O}	2.443	2.418	2.447	2.422	2.451	2.425	2.496	2.224
θ_{O-U-O}	175.8	176.5	176.0	176.2	178.3	178.4	179.8	175.0
$\theta_{CO-U-ON}$	64.9, 65.6	65.5, 66.4	65.2, 65.8	65.7, 66.6				
$\theta_{CO-U-OC}$					53.5, 54.2	54.1, 54.7		
$\lvert\theta_{NO-U-OC-C}\rvert$	2.9, 9.7	6.1, 9.9	7.4, 8.7	8.0, 8.6				
$\lvert\theta_{N-C-C-CH}\rvert$	0.7, 1.7	0.8, 1.9	25.9, 26.0	25.9, 26.2				
n_f	2.51	2.06	2.51	2.03	2.54	2.09		

[a] Interatomic distances and angles are given in Å and deg., respectively.

claim of Boulet et al.[18] that, for the very similar 2-methoxyethanehydroxamate system $[UO_2(\eta^2\text{-}CH_3OCH_2CONHO)_2]$, the preferred equatorial coordination number is 6, i.e., that the microsolvated species is $[UO_2(\eta^2\text{-}CH_3OCH_2CONHO)_2(OH_2)_2]$. This is because Boulet et al.'s stability criterion is based on total energies with respect to dissociation to independent UO_2^{2+}, $CH_3OCH_2CONHO^-$, and OH_2 fragments only. In terms of this stability criterion we also find $[UO_2sha_2(OH_2)_2]$ to be more stable than $[UO_2sha_2OH_2]$ by ca. 14.2 kJ mol^{-1}, with gas-phase binding energies of 2445.5 and 2459.7 kJ mol^{-1}, respectively. But the gas-phase binding energy of 2482.6 kJ mol^{-1} of the competing $[UO_2sha_2OH_2\cdot OH_2]$ is even larger; that is, the second OH_2 ligand prefers the second UO_2^{2+} solvation sphere by 22.9 kJ mol^{-1}. (Actually, the LPP binding energies of 2484.9, 2497.5, and 2524.8 kJ mol^{-1} compare more directly to Boulet et al.'s large-core pseudopotential calculations.) We note that our considerations are, to some extent, limited, as routine DFT methods tend to overestimate OH_2-OH_2 interactions with respect to metal ion$-OH_2$ interactions[40a,b] and typically provide only poor models for dispersion interactions, thus biasing versus smaller preferred hydration numbers x' systematically.[40c−e] However, we believe that our stability criterion is superior to that of Boulet et al.,[18] who do not consider any competition between the first and second UO_2^{2+} solvation sphere at all, while the second OH_2 ligand prefers the outer UO_2^{2+} solvation sphere by 10.3 kJ mol^{-1} at the RI-MP2 level of theory. We therefore limit the following discussion to the η^2-[O,O] *anti*-$[UO_2L_2OH_2]$ class of systems.

As discussed for the parent $[UO_2L_2]$ systems, mean apical U−O distances d_{U-O} are largely independent of L^-, differing by 0.010 Å at most (cf. Table 3). With respect to $[UO_2L_2]$, the extra OH_2 ligand causes d_{U-O} elongations of only 0.004, 0.002, and 0.004 Å for the sha, bha, and ba system, respectively; compared to $[UO_2(OH_2)_5]^{2+}$ with d_{U-O} = 1.749 Å, apical U−O distances are larger by 0.035, 0.034, and 0.025 Å. Whereas from the symmetry breaking due to the extra OH_2 ligand d_{CO-U} and d_{NO-U} are slightly different for both L^- ligands in $[UO_2L_2OH_2]$, both are similar for sha^- and bha^-; the CO−U distance appears to be more sensitive to the nature of L^-, being consistently larger by 0.010 Å for bha^- than for sha^-. Again, the ba system's mean equatorial d_{U-O} of 2.451 Å is in between the individual hydroxamate U−O, but larger than the mean hydroxamate U−O distances of 2.443 and 2.447 Å for the sha and bha system, respectively. U$-OH_2$ distances of 2.600, 2.594, and 2.554 Å are generally larger than L^- U−O distances. All interatomic distances agree with $[UO_2(\eta^2\text{-}CH_3OCH_2CONHO)_2OH_2]$ mean U−OC, U−ON, and U$-OH_2$ distances and mean equatorial U−O distances of 2.435, 2.576, and 2.463 Å, respectively, by Boulet et al.[18] Interestingly the sha^- and bha^- mean tilt angles $|\theta_{NO-U-OC-C}|$ of only 6.3° and 8.1° are significantly smaller than found for the parent $[UO_2L_2]$ systems; Boulet et al. find mean tilt angles of 3.3°.[18] L^- bite angles θ are 65.3°, 65.5°, and 54.4° for the sha, bha, and ba system, respectively, and thus show the same global trend as discussed for the parent $[UO_2L_2]$ systems; Boulet et al. find mean bite angles θ of 65.2° for $[UO_2(\eta^2\text{-}CH_3OCH_2CONHO)_2OH_2]$.[18]

Compared to experimental EXAFS data, calculated $[UO_2L_2OH_2]$ structure parameters match their experimental counterparts much better than the $[UO_2L_2]$ ones. Mean apical U−O distances of 1.784 and 1.783 Å differ by less than 0.01 Å from the EXAFS values of 1.78 and 1.77 Å for sha and bha, respectively. Mean equatorial U−O distances of 2.443 and 2.447 Å match the EXAFS values of 2.42 and 2.40 Å with excellent agreement, although, within the experimental error of ca. 0.01 Å, give the opposite trend. However, averaging over the structure parameters of $[UO_2(OH_2)_5]^{2+}$,[21] $[UO_2L(OH_2)_3]^+$,[21] and $[UO_2L_2OH_2]$, with weights according to the EXAFS samples' composition given in Table 1, weighted average apical U−O distances of 1.779 and 1.778 Å and weighted average equatorial U−O distances of 2.451 and 2.449 Å for sha and bha, respectively, compare excellently and recover the same trend as observed experimentally. The systematic overestimation of equatorial U−O distances by a few picometers is known to stem from our limited solvation model and is well systematically improvable by relaxing molecular structures in the COSMO potential.[41a−c]

(40) (a) Tsushima, S. *J. Phys. Chem. A* **2007**, *111*, 3613–3617. (b) Wiebke, J.; Moritz, A.; Cao, X.; Dolg, M. *Phys. Chem. Chem. Phys.* **2007**, *9*, 459–465. (c) Austin, J. P.; Burton, N. A.; Hillier, I. H.; Sundararajan, M.; Vincent, M. A. *Phys. Chem. Chem. Phys.* **2009**, *11*, 1143–1145. (d) Wåhlin, P.; Danilo, C.; Vallet, V.; Réal, F.; Flament, J.-P.; Wahlgren, U. *J. Chem. Theory Comput.* **2008**, *4*, 569–577. (e) Cao, Z.; Balasubramanian, K. *J. Chem. Phys.* **2009**, *131*, 164505-1–164505-12. (f) Paizs, B.; Suhai, S. *J. Comput. Chem.* **1998**, *19*, 575–584.

(41) (a) Ingram, K. I. M.; Häller, L. J. L.; Kaltsoyannis, N. *Dalton Trans.* **2006**, *20*, 2403–2414. (b) Yang., T.; Bursten, B. E. *Inorg. Chem.* **2006**, *45*, 5291–5301. (c) Cao, Z.; Balasubramanian, K. *J. Chem. Phys.* **2005**, *123*, 114309-1–114309-12.

Table 4. Calculated B3LYP-DFT $[UO_2L_2(OH_2)_y]$ Gas-Phase Binding Energies ΔE_y, Given in kJ mol^{-1}, from the SPP and LPP Computational Scheme, and Experimental TRLF Spectroscopic Stability Constants log β from Aqueous Solution[20]

	$[UO_2sha_2(OH_2)_y]$		$[UO_2bha_2(OH_2)_y]$		$[UO_2ba_2(OH_2)_y]$	
	SPP	LPP	SPP	LPP	SPP	LPP
ΔE_0	2394.3	2427.9	2362.3	2395.5	2243.8	2274.9
ΔE_1	2445.5	2484.9	2414.4	2455.1	2306.9	2345.0
log β	35.0		16.07			

Again, the LPP computational scheme gives the same global picture as discussed above. U-involving interatomic distances are consistently smaller than the SPP values, with maximum deviations of interatomic distances $d \leq 2.75$ Å of 0.048, 0.048, and 0.049 Å for the sha, bha, and ba systems, respectively; angular parameters deviate by at most 3.0°, 1.8°, and 1.5° from the SPP values, but less systematically. Again, ligand-related structure parameters, such as dihedral angles, are largely unaffected.

4.3. Gas-Phase Relative Stabilities. Table 4 lists zero-point-corrected gas-phase binding energies

$$\Delta E_y = E([UO_2L_2(OH_2)_y]) - E(UO_2^{2+}) - 2E(L^-) - yE(H_2O)$$

for $y = 0$ and $y = 1$, where E(X) is the B3LYP-DFT total energy of fragment X plus X's scaled zero-point vibrational energy. Note that from our computational approach one cannot come to relative stabilities for aqueous solution, since, for example, $E'([UO_2L_2(OH_2)_y]) + (5 - y)E'(H_2O) - 2E'(L^-) - E'([UO_2(OH_2)_5])$, with E'(X) including the COSMO energy contribution, lacks discrete L^- solvation on the reactant side of the ligand substitution reaction, thus giving too large energy differences.

The gas-phase binding energies ΔE_0 of 2394.3, 2362.3, and 2243.8 kJ mol^{-1} for the sha, bha, and ba systems, respectively, show the same general trend as gas-phase binding energies of 1649, 1616, and 1510 kJ mol^{-1} for the analogous $[UO_2L]^+$ sha, bha, and ba systems[21] and as TRLF spectroscopic stability constants[20] log β of 35.0 and 16.07 for the 1:2 sha and bha systems. $[UO_2sha_2]$ is more stable than $[UO_2bha_2]$ by 32.0 kJ mol^{-1}, but more stable than $[UO_2ba_2]$ by 150.5 kJ mol^{-1}, which suggests a greater affinity of UO_2^{2+} to the hydroxamato as compared to the carboxylato ligand, as established by Boulet et al.[18] from similar considerations. Within the LPP computational scheme, gas-phase binding energies ΔE_0 of 2427.9, 2395.5, and 2274.9 kJ mol^{-1} are systematically larger by ca. 30 kJ mol^{-1} (i.e., by at most 33.6 kJ mol^{-1} or 1.4% for the sha system) and, thus, give precisely the same picture.

We note in passing that our B3LYP-DFT gas-phase binding energies ΔE_0 are probably systematically too small due to the UO_2^{2+}−ligand interaction's dispersion component, which is not properly accounted for by B3LYP-DFT.[40c−e] Indeed, the single-point RI-MP2 ΔE_0 of the $[UO_2sha_2]$ example is larger; that is, the ZPE-uncorrected value is 2543.7 kJ mol^{-1}, yielding 2529.7 kJ mol^{-1} after adding a B3LYP-DFT ZPE correction. However, since MP2 is known to be much more sensitive to basis set superposition errors (as discussed by, for example, Paizs and Suhai[40f]) and, thus, to give too large binding energies, this result might not be more accurate than the DFT one.

4.4. Experimental UV−Vis and Calculated Excitation Spectra. Both the sha and bha 1:2 systems' experimental UV−vis spectra from aqueous solution, recorded in the 350−460 nm range, and calculated B3LYP-TD-DFT excitation spectra for $[UO_2sha_2OH_2]$ and $[UO_2bha_2OH_2]$ are given in the Supporting Information; the experimental absorption maxima and calculated excitation energies at the B3LYP-TD-DFT, RI-CIS, and RI-CIS(D) levels of theory are given in Table 5.

Experimentally, the sha and bha 1:2 systems' UV−vis spectra show one single broad absorption band at 390 and 386 nm, respectively, and are thus very similar. Both absorption bands are indicative for complex formation in the sense that superpositions of the fragment, i.e., the UO_2^{2+} and L^- UV−vis spectra, lack this feature. Note that the sha and bha 1:1 systems' UV−vis spectra[18,21] are also very similar, each exhibiting a single broad absorption band at 402 and 401 nm, respectively. Similar to the analogous $[UO_2sha(OH_2)_3]^+$ and $[UO_2bha(OH_2)_3]^+$ case,[21] calculated B3LYP-TD-DFT excitation spectra show three groups of transitions differing in both wavelengths λ and relative intensities: large-intensity $UO_2^{2+} \leftarrow OH_2$ charge-transfer (CT) excitations with $\lambda \leq 200$ nm, L^- $\pi^* \leftarrow \pi$ excitations of intermediate intensities in the 200−300 nm range, and $UO_2^{2+} \leftarrow L^-$ CT excitations of low intensities in the 300−700 nm range. Whereas the calculated $[UO_2sha_2OH_2]$ absorption maximum at 395 nm seemingly matches its experimental counterpart at 390 nm, that calculated for the $[UO_2bha_2OH_2]$ system is blue-shifted by 54 nm or 0.52 eV with respect to the experimental data (cf. Supporting Information). Clearly, from the spin−orbit stabilization of the U^V-O_2^+ $^2\Phi_u$ state by ca. 0.3−0.4 eV,[42a,b] $UO_2^{2+} \leftarrow L^-$ CT excitations into UO_2^{2+} 5f atomic orbital-like molecular orbitals might be overestimated by a similar, but (from quenching by the L^- and OH_2 ligand field) somewhat smaller amount since our scalar-relativistic computational scheme does not address spin−orbit splitting. However, from the overall similarity of the $[UO_2sha_2OH_2]$ and $[UO_2bha_2OH_2]$ systems one may safely assume comparable performance of a given computational scheme and, thus, infer that the sha system's experimental UV−vis and calculated B3LYP-TD-DFT spectra match for the wrong reason. It is, instead, much more consistent to assign the sha and bha systems' calculated $UO_2^{2+} \leftarrow L^-$ CT excitations at ca. 550−620 nm to the experimentally observed absorption bands. It is known that, for CT transitions, TD-DFT is sometimes not reliable and can give much too small excitation energies.[43] The RI-CIS and RI-CIS(D) model excitation energies given in Table 5, which do not suffer from the B3LYP-TD-DFT asymptotic error,[44] indicate that here and in our previous study of the analogous 1:1 systems[21] B3LYP-TD-DFT excitation energies are signficantly

(42) (a) Ruipérez, F.; Danilo, C.; Réal, F.; Flament, J.-P.; Vallet, V.; Wahlgren, U. *J. Phys. Chem. A* **2009**, *113*, 1420–1428. (b) Hay, J. P.; Martin, R. L.; Schreckenbach, G. *J. Phys. Chem. A* **2000**, *104*, 6259–6270.

(43) Dreuw, A.; Weisman, J. L.; Head-Gordon, M. *J. Chem. Phys.* **2003**, *119*(6), 2943–2946.

(44) Cao, X.; Dolg. M. Relativistic Pseudopotentials. In *Relativistic Methods for Chemists*; Barysz, M.; Ishikawa, Y., Eds.; Springer: Berlin, 2009.

(45) Puigdomenech, I. *Input, Sed, and Predom: Computer Programs Drawing Equilibrium Diagrams*; TRITA-OOK-3010, RIT: Stockholm, 1983.

Table 5. Largest Four Calculated B3LYP-TD-DFT, RI-CIS, and RI-CIS(D) Excitation Wavelengths for the $[UO_2sha(OH_2)_3]^+$, $[UO_2bha(OH_2)_3]^+$, $[UO_2sha_2OH_2]$, and $[UO_2bha_2OH_2]$ Systems and Experimental UV−Vis Absorption Maxima, Given in nm

	$[UO_2sha(OH_2)_3]^+$	$[UO_2bha(OH_2)_3]^+$	$[UO_2sha_2OH_2]$	$[UO_2bha_2OH_2]$
B3LYP-TD-DFT	683, 678, 624, 608	674, 668, 615, 598	624, 617, 608, 600	620, 613, 607, 596
RI-CIS	290, 282, 281, 279	289, 281, 280, 279	287, 281, 279, 277	287, 281, 279, 276
RI-CIS(D)	346, 338, 346, 353	342, 334, 343, 348	342, 317, 346, 350	340, 318, 345, 347
exptl	393	390	390	386

underestimated. Therefore, $UO_2^{2+} \leftarrow L^-$ CT transitions calculated to be in the experimental 350−460 nm range for $[UO_2sha(OH_2)_3]^+$, $[UO_2bha(OH_2)_3]^+$, and $[UO_2sha_2OH_2]$, but not for $[UO_2bha_2OH_2]$, must be regarded as higher, i.e., near-UV, CT transitions, being red-shifted from insufficiencies of our computational protocol.

4.5. Remarks on the Performance of the Computational Models. As already discussed in much more detail in the preceding sections, one can conclude that the LPP approximation[23] can be applied with the very same success as the SPP approximation when it comes to the consideration of molecular structures and gas-phase binding energies of the $[UO_2L_2(OH_2)_y]$ systems. Deviations of LPP from SPP structure parameters are generally a few picometers and degrees only, and LPP and SPP gas-phase binding energies ΔE typically differ by ca. 1−2%. Furthermore, the LPP clearly is more efficient than the SPP approximation: Within our general computational protocol, LPP and SPP B3LYP-DFT single-point energy calculations on UO_2^{2+} take ca. 47 and 78 s on an Intel Core2 Quad machine (3 GHz, 4 GB RAM), respectively, starting from a null-density guess. (Note that the computing time per self-consistent-field iteration is even more favorable for the LPP computational scheme, as the LPP and SPP calculations take 48 and 23 iterations, respectively, using the TURBOMOLE nondefault setting \$scfdamp start = 1.00 step = 0.10 min = 0.10.) The success of the LPP approximation to the $[UO_2L_2(OH_2)_y]$ can be explained by the sufficiently small deviations between LPP and SPP 5f occupations of at most 0.48 electron (cf. Table 3). Consequently, it is for this reason that the LPP approximation breaks down when it comes to the consideration of molecular properties that involve the 5f shell directly, e.g., excitation energies for $UO_2^{2+} \leftarrow L^-$ CT transitions: Although the LPP's f-part allows for some additional 5f occupation,[23] larger deviations from the U^{VI} $5f^0$ case, e.g., from $UO_2^{2+} \leftarrow L^-$ CT excitations, give rise to large frozen-core errors[44] and deteriorate the excitation spectrum.

5. Conclusion

Our recent[21] and present combined experimental and theoretical investigation provide a consistent picture of the coordination chemistry of U^{VI}, i.e., UO_2^{2+}, and salicylhydroxamate, benzohydroxamate, and benzoate in aqueous solution. Considering UO_2^{2+}−hydroxamate systems with UO_2^{2+}-to-ligand ratios of 1:2, the UO_2^{2+} equatorial coordination number is ca. 5, and mean equatorial U−O distances are 2.42 and 2.40 Å for the sha and bha systems, respectively, from U L(III) edge EXAFS spectroscopy. B3LYP-DFT calculations indicate that η^2-[O,O] *anti*-$[UO_2sha_2OH_2]$ and -$[UO_2bhaOH_2]$ are the most reasonable representations of the systems observed experimentally. The molecular structure parameters averaged according to the EXAFS samples compositions from the free UO_2^{2+} and 1:1 and 1:2 sha and bha systems, i.e., mean apical U−O distances of 1.779 and 1.778 Å and mean equatorial U−O distances of 2.451 and 2.449 Å for the sha and bha systems, respectively, deviate by at most 0.05 Å from experimental EXAFS data. The overestimation of calculated equatorial U−O distances is systematic and known to stem from the limitations of the hybrid-type solvation model applied, i.e., from neglecting bulk solvation effects on molecular structure parameters. In line with experimental stability constants,[19,20] B3LYP-DFT gas-phase binding energies decrease from sha^- via bha^- to ba^-; $[UO_2sha_2]$ is more stable than $[UO_2bha_2]$ and $[UO_2ba_2]$ by 32.0 and 150.5 kJ mol^{-1}, respectively, suggesting a greater affinity of UO_2^{2+} to the hydroxamate than to the carboxylate ligands. Comparing the two different pseudopotential (U small-core and large-core, i.e., SPP and LPP) computational schemes applied suggests that it is perfectly safe within the systematic errors of both experiment and theory to apply the more efficient LPP approximation[23] (when not considering molecular properties that involve the 5f shell directly, e.g., excitation energies for $UO_2^{2+} \leftarrow L^-$ CT transitions).

Both the sha and bha 1:2 systems' experimental UV−vis spectra from aqueous solution are dominated by one single absorption band with λ maxima of 390 and 386 nm, respectively. As indicated by RI-CIS and RI-CIS(D) model calculations, B3LYP-TD-DFT significantly underestimates $UO_2^{2+} \leftarrow L^-$ CT excitation energies from its inherent asymptotic error and, thus, cannot be regarded as a reliable computational scheme for the calculation of excitation spectra of the systems under investigation.

Acknowledgment. The financial support of the Deutsche Forschungsgemeinschaft (DFG) to J.W. and A.W. is gratefully acknowledged. The experimental work was funded by the BMWi under contract number 02E9985. EXAFS measurements were done at BM20 (ROBL) at the ESRF. We thank A. Rossberg, H. Funke, C. Hennig, and A. Scheinost for their help and support during the XAS experiments at ROBL. Futhermore, we wish to thank ACTINET, particularly J.-P. Flament, N. Kaltsoyannis, B. Schimmelpfennig, and V. Vallet, for providing an inspiring and encouraging atmosphere at the ACTINET ThUL School 2006 in Lille, where the current joint research project was initiated.

Supporting Information Available: Initial and DFT-optimized molecular structure Cartesian coordinates; DFT total and vibrational zero-point energies; experimental UV−vis spectra of the U^{VI} sha and bha systems in aqueous solution, and calculated B3LYP-TD-DFT excitation spectra of $[UO_2sha_2OH_2]$ and $[UO_2bha_2OH_2]$. This material is available free of charge via the Internet at http://pubs.acs.org.